

Lawrence Berkeley National Laboratory

LBL Publications

Title

Getters for improved technetium containment in cementitious waste forms

Permalink

<https://escholarship.org/uc/item/7293m6nx>

Authors

Asmussen, R Matthew

Pearce, Carolyn I

Miller, Brian W

et al.

Publication Date

2018

DOI

10.1016/j.jhazmat.2017.07.055

Peer reviewed

1 Getters for Improved Tc Containment in Cementitious Waste Forms

2 R. Matthew Asmussen¹, Carolyn I. Pearce¹, Brian D. Miller¹, Amanda R. Lawter¹, James J.
3 Neeway¹, Wayne W. Lukens², Mark Bowden¹, Micah Miller¹, R. Jeffery Serne¹, Nikolla P.
4 Qafoku¹

5 ¹Pacific Northwest National Laboratory, Richland, WA

6 ²Chemical Sciences Division, Lawrence Berkeley National Laboratory, Berkeley, CA

7 **Keywords** : nuclear waste management, technetium, getters, cementitious, grout, radiography,
8 spectroscopy

9

10

11 **Abstract**

12

13 Cementitious waste forms present a low-temperature, low-cost option for the immobilization of
14 nuclear wastes. At the U.S. Department of Energy Hanford Site, the low activity waste (LAW)
15 portion of the nuclear wastes stored at the site will contain Tc-99, a long lived radionuclide
16 capable of high environmental mobility. A cementitious waste form known as Cast Stone is
17 under investigation as a possible candidate technology for the immobilization of LAW. Ensuring
18 slow rates of release of Tc from a LAW waste form, be it glass or cementitious, is essential for
19 safe disposal of the waste. This work focuses on the addition of getter materials to Cast Stone
20 that can selectively immobilize Tc from the LAW, and in turn, lower Tc release from the Cast
21 Stone. Two getters which produce different products upon sequestering Tc from LAW were
22 tested in Cast Stone; Sn(II)-treated apatite (Sn-A) which removes Tc as a Tc(IV)-oxide and
23 potassium metal sulfide (KMS-2) which removes Tc as a Tc(IV)-sulfide species. The Cast Stone
24 treated with KMS-2 had the largest impact. The observed diffusion (D_{obs}) of Tc decreased from
25 $4.6 \pm 0.2 \times 10^{-12} \text{ cm}^2/\text{s}$ for Cast Stone that did not contain a getter to $5.4 \pm 0.4 \times 10^{-13} \text{ cm}^2/\text{s}$ for
26 KMS-2 containing Cast Stone, where KMS-2 addition was equivalent to $< 0.01 \text{ wt}\%$ of the total
27 waste form mass. The Sn-A Cast Stone also improved Tc D_{obs} over time, however initial releases
28 were higher due to the higher level of Sn-A addition required ($\sim 2 \text{ wt}\%$ overall). Spectroscopic
29 investigations using single particle digital autoradiography and μ -X-ray fluorescence determined
30 Tc to remain associated with the getter materials within the Cast Stone matrix. It was found that
31 Tc-sulfide species are more stable within Cast Stone compared with Tc-oxides using x-ray
32 absorption spectroscopy (XAS). This stable state of Tc produced by the KMS-2 is the origin of
33 the decrease in Tc D_{obs} . From this result, sulfide-containing materials should be further
34 investigated to help improve Cast Stone performance (or any other cementitious material).

35

36

1. Introduction

37 One of the greatest challenges facing the world today is the development of a secure,
38 low-carbon energy supply. Nuclear power a well-developed technology with a potential to play a
39 key role in such development. Public discussion about nuclear power has focused on the long-
40 term management and disposal of radioactive waste, a by-product from energy and weapons
41 production, the majority of which is currently kept in temporary storage although some low level
42 waste repositories are in operation around the globe. Thus, the future development of nuclear
43 power is critically dependent on bringing closure to the fuel cycle, with the assurance of safe,
44 long-term storage of used fuel and all resulting nuclear waste, including legacy waste. Liquid
45 nuclear wastes are generated from processing of used nuclear material and are currently included
46 in the nuclear inventory of several countries including the United States, Japan, France, the
47 United Kingdom, Canada ¹, and Germany ². Vitrification to produce a borosilicate glass (or
48 alumino-phosphate glass in Russia) ³ is the baseline technology for immobilization of radioactive
49 liquid wastes, owing to the long-term chemical stability of glass. However, vitrification requires
50 high temperatures (> 1000 °C) and certain radionuclides, including technetium-99 (Tc) ⁴ and
51 iodine-129 (I), ⁵ are highly volatile at such temperatures. The result is limited incorporation of
52 the volatile radionuclides into the final waste form and generation of secondary waste streams
53 that require additional immobilization and management.

54 The challenge of immobilization of liquid nuclear wastes containing volatile
55 radionuclides is best exemplified by the environmental clean-up mission currently ongoing at the
56 U.S.A. Department of Energy (DOE) Hanford site, located in southeastern Washington, U.S.A.
57 Nine reactors at the Hanford site produced 67 tons of plutonium from 1943-1989 ⁶. As a result
58 of the Pu production, a large inventory of radioactive wastes with widely different compositions
59 were generated. Fifty-six million gallons of the waste currently remain stored in 177 storage
60 tanks at the site ⁷. Initially, waste tanks were comprised of a single carbon steel shell, which
61 began to leak in 1959 due to the corrosive nature of the wastes ⁸. In total, 67 of the 149 single
62 shell tanks have leaked and the drainable and pumpable liquid waste has now been transferred to
63 more robust double shell tanks. However, the double shell tanks themselves are now
64 approaching the end of their design life and the first leak from a primary tank into the secondary
65 liner of a double-shell tank has recently been discovered ⁹. Thus, it is imperative that these
66 wastes be removed from the tanks and immobilized in a timely manner.

67 Current management plans of the Hanford tank wastes calls for separated into high-level
68 (high radioactivity and low volume, HLW) and low-activity (high radioactivity and lower
69 volume, LAW) waste streams. The waste streams will be vitrified at the Hanford Tank Waste
70 Treatment and Immobilization Plant (WTP). Much of the technetium is expected to volatilize out
71 of the molten glass and become trapped in the gas scrubber. Given the volume of LAW to be
72 treated at WTP, and the generation of secondary waste streams, including the aqueous solution
73 from the gas scrubber, alternate solidification technologies are being investigated to assist in the
74 clean-up mission. Cementitious waste forms present suitable characteristics for treating Tc

75 containing wastes as their fabrication temperatures are below the volatility point of Tc and their
76 low fabrication costs are favorable for immobilizing large volumes of waste. Cementitious waste
77 forms are currently used for the immobilization of liquid wastes at the DOE Savannah River site,
78 ^{10,11} at other global waste treatment sites for low level wastes, ¹² and under consideration as an
79 immobilization technology in several countries ^{13,14}. The most prominent issue influencing the
80 use of cementitious waste form technologies is the ability to demonstrate that the retention of
81 radionuclides of concern, such as Tc, is sufficient to ensure insignificant environmental impact
82 from the waste disposal.

83 The environmental risk associated with Tc release from immobilized waste forms is high
84 due to the long half-life of Tc (213,000 years) and its high mobility in subsurface environments.
85 In oxidizing environments, Tc primarily exists in an oxyanion form, pertechnetate (TcO_4^-). TcO_4^-
86 has limited adsorption onto many common minerals including silicates, carbonates and sulfates
87 (e.g. biotite, apatite, dolomite and gypsum) from the aqueous phase ^{15,16}. As a result, TcO_4^- in
88 groundwater will migrate rapidly under oxic conditions, irrespective of the biogeochemistry,
89 climate, and physical characteristics of the site ^{17,18}. At the Hanford site, a significant Tc plume
90 exists in the subsurface ¹⁹ resulting from the tank leaks. Given this unhindered migration
91 through the subsurface, any release of Tc from a waste form must be kept to a minimum.

92 At the Hanford site, both glass and cementitious waste will be stored at the Integrated
93 Disposal Facility (IDF). The IDF is a landfill design which measures 457 m × 233 m × 13 m
94 (from the surface) and was constructed in 2006, although has not accepted any waste to date.
95 The projected volume of immobilized LAW to be generated exceeds the current expected
96 capacity of the vitrification facilities. To overcome this limitation, Cast Stone, a cementitious
97 waste form comprised of a dry mix of 47 wt% blast furnace slag, 45 wt% fly ash and 8 wt%
98 ordinary Portland cement, is currently being considered as a possible candidate waste form to
99 provide additional LAW immobilization capacity ^{20,21}.

100 Investigations to determine the optimum dry to wet mix ratio of Cast Stone with various
101 LAW simulants, containing a combination of Tc, I, and U spikes, were conducted previously
102 using EPA Method 1315 leach testing ^{22,23}. The EPA Method 1315 test involves placing a
103 monolithic sample into a leachant at a surface area to volume ratio of 1 cm² : 9 mL for a set
104 interval duration, after which the monolith is removed and placed into fresh leachant and
105 repeated ²³. From these investigations, it was determined that Cast Stone had promising
106 properties for retention of Tc, although release was influenced by variations in the Cast Stone
107 composition ²⁰. It was concluded that retention of radionuclides by the Cast Stone, and
108 cementitious waste forms in general, may be improved through the inclusion of materials which
109 can selectively sequester radionuclides or contaminants of interest in both the liquid state and
110 final waste form, termed getters ²⁴.

111 A range of getter materials that target and sequester Tc from aqueous media has been
112 investigated in the scope of nuclear research, including metal oxides ²⁵, nanomaterials ^{26,27},

113 carbon-based materials²⁸, aluminophosphates²⁹, and resins^{30,31}. Many of these materials
114 showed promise for the removal of Tc from chemically inert aqueous environments at
115 circumneutral pH and with low ionic strengths³²⁻³⁴. However, a drastic drop in performance was
116 observed with many Tc getters upon moving to extreme chemical environments with high ionic
117 strength, high/low pH and presence of competitive redox-active species. These more extreme
118 conditions are relevant to removal of Tc from LAW because it has a high pH (> 13), high ionic
119 strength (between 5 M and 8 M Na), and contains high levels of redox-active species, such as
120 Cr(VI) and NO₃⁻. Two getter materials have recently shown high promise for the removal of Tc
121 from chemically complex environments, including LAW: Sn(II)-treated apatite (Sn-A)³⁵ and
122 layered potassium metal sulfide (KMS-2)³⁶. Although the mechanisms vary, both the Sn-A and
123 KMS-2 sequester Tc from solution through reduction of Tc(VII) to Tc(IV). The Sn-A sequesters
124 Tc as a Tc(IV)-oxide and KMS-2 as a Tc(IV)-sulfide. These Tc(IV) species have far lower
125 solubility than Tc(VII) species, which decreases Tc mobility.

126 Both Sn-A and KMS-2 are suitable candidates to be used as Tc getters incorporated into
127 Cast Stone or other cementitious waste forms based on previous testing. Here, we present for the
128 first time the process of fabrication, followed by rigorous testing and thorough characterization
129 of the Cast Stone waste form containing either Sn-A or KMS-2 as a Tc getter for solidification of
130 a representative chemically extreme (i.e., high pH and ionic strength) LAW simulant. By using
131 the two getters, a comparison between the stability of two forms of Tc(IV) can be made upon
132 introduction to a cementitious waste form. EPA method 1315 leach testing was conducted using
133 simulated Hanford vadose zone pore water, which is the likely contacting solution for a waste
134 form placed at the IDF. Advanced solid phase characterization techniques including x-ray
135 absorption spectroscopy (XAS), micro-x-ray fluorescence (μ -XRF), and novel single-particle
136 digital autoradiography (iQid) were used. These techniques, in combination with the results from
137 the XRD analyses and leachate concentrations, provide insights into Tc molecular associations in
138 Cast Stone and aid in the understanding of mechanisms and pathways that control Tc release
139 from getter-containing Cast Stone.

140 **2. Experimental Details**

141 ***2.1 Solution Preparation***

142 *2.1.1 Low Activity Waste Simulant*

143 The Cast Stone samples in this study were prepared using a LAW simulant with an
144 average target Na content of 6.5 M. This LAW simulant is based on the Hanford Tank Waste
145 Operations Simulator (HTWOS) model, which supports the River Protection Project System Plan
146 Revision 6³⁷. The composition of the LAW simulant is given in Table 1. Distilled deionized
147 water (DDI, 18.2 M Ω ·cm) was used and the chemicals (Sigma-Aldrich or Fisher Scientific) were
148 added in the order given in Table 1. Each chemical was added individually while the simulant
149 was being stirred; the compound was allowed to fully dissolve prior to adding the next one.. If

150 required, the simulant was heated to ~ 70 °C to facilitate chemical dissolution. After the addition
 151 of the final chemical, the simulant was stirred and cooled for ~ 16 h before DDI was added to
 152 reach the target mass. The measured composition of the LAW simulant after fabrication is also
 153 listed in Table 1. The long term leached Cast Stone sample presented in this work was fabricated
 154 with a similar LAW simulant with a Na concentration of 8.3 M.

155 Table 1 - Composition of the LAW Simulant utilized in Cast Stone formation.

Compound	Amount for 1 L (g)	Anion/Cation	Measured Concentration (g/L)	Concentration (mol/mol Na)
DDI	200 mL	Na	153.33	1.000
KNO ₃	4.60	Al	11.75	0.065
NaCl	3.04	Cl	3.47	0.015
NaF	1.64	NO ₃	140.00	0.339
Na ₂ SO ₄	15.70	NO ₂	37.04	0.121
Al(NO ₃) ₃ •9H ₂ O	148.74	SO ₄	11.58	0.018
NaOH (50% soln)	289.12	K	2.08	0.008
Na ₃ PO ₄ •12H ₂ O	24.71	PO ₄	1.47	0.002
NaC ₂ H ₃ O ₂	6.64	Free OH	35.39	0.312
Na ₂ CO ₃	37.89			
DDI	100 mL			
Na ₂ Cr ₂ O ₇ •2H ₂ O	2.31			
DDI	100 mL			
NaNO ₃	74.03			
NaNO ₂	50.68			
DDI	100 mL			

156

157 The LAW simulant was spiked with Tc using a 10 400 ppm NaTcO₄ stock solution to a
 158 target spike of 16 ppm, and with I using a 10 000 ppm NaI stock solution to a target spike of 5
 159 ppm (only the results for Tc will be described in this paper). The HTWOS model predicts a Tc
 160 concentration of 4.6 ppm for a 6.5 M Na concentration, thus the 16 ppm spike level is ~ 3.5
 161 times the predicted HTWOS value and allows for comparison to previous Cast Stone tests using
 162 a similar Tc content. The long-term leached Cast Stone samples analyzed in this report were
 163 spiked with 56 ppm Tc (10 × the Tc concentration predicted by HTWOS for a LAW simulant
 164 with a Na concentration of 7.8 M) to aid in ability to detect Tc in solid state analytics.

165 *2.1.2 Hanford Vadose Zone Porewater*

166 The simulated Hanford vadose zone pore water (VZPW) used for leach testing (Table 2) was
167 developed based on several measurements of actual VZPW removed from a borehole of Hanford
168 formation sediments where the IDF is located³⁸. A large field sample of moist sediment was
169 removed from Hanford formation sediments using cable tool drive barreling. The field moist
170 sediments were then ultra-centrifuged for several hours. Small volumes of solution were passed
171 through the sediment and collected. When approximately 30 to 50 mL of solution was collected
172 from each sediment sample it was immediately filtered through 0.45 µm membrane filters and
173 analyzed for chemical composition. The results from characterizing the pore water from two
174 depths (48.5 and 82.5 feet below ground surface) from a borehole from the IDF location
175 (specifically borehole C4124; 299-E27-22)³⁸ were averaged and charge balanced. Reagents were
176 added, in the order given in Table 2, to the corresponding volume of distilled water.

177 Table 2 - Composition of the simulated Hanford vadose zone pore water (VZPW) used in EPA
178 Method 1315 leach testing.

VZPW Recipe			
Order	Molarity (mol/L)	Reagents	g/L
1	0.012	CaSO ₄ •2H ₂ O	2.07
2	0.0017	NaCl	0.10
3	0.0004	NaHCO ₃	0.03
4	0.0034	NaNO ₃	0.29
5	0.0026	MgSO ₄	0.31
6	0.0024	MgCl ₂ •6H ₂ O	0.49
7	0.0007	KCl	0.05
Adjust pH to 7.0 (±0.2) with sodium hydroxide or sulfuric acid dependent on initial pH.			

179

180 *2.2 Cast Stone Fabrication*

181 *2.2.1 Selection of Tc Getters*

182 Two Tc getters were selected for Cast Stone fabrication based on previous work. Sn(II)-
183 treated apatite (Sn-A), fabricated as described in Asmussen et al.³⁵, was selected based on its
184 ability to reduce Tc(VII) to Tc(IV) and produce a Tc(IV)O₂ · x H₂O final product³⁵. The likely
185 chemical formula is Ca_{x-y}Sn_y(PO₄)_x(X), where X is the supporting anion being either OH, F or
186 Cl. The Sn-A used in this study has a reduction capacity of 3469 ± 530 microequivalents (µeq)
187 of electrons/g³⁵ measured using the Ce(IV) reduction capacity method³⁹. Sn-A has shown
188 preferential reduction of Cr(VI) over Tc(VII) and is deleteriously affected by high alkaline
189 environments³⁵. To assure maximum aqueous Tc removal, the mass of added Sn-A (i.e., 50 g)
190 was theoretically capable of reducing ~ 3 times the Cr(VI) content and 10 times the Tc content of
191 the LAW simulant.

192 Potassium metal sulfide (KMS-2) was developed as a material for removing hazardous
 193 cationic species from different solutions^{40,41}. KMS-2 has also shown the highest performance of
 194 Tc(VII), as TcO_4^- , removal from LAW³⁶. The KMS-2 used in this report was fabricated using
 195 the solid state approach described in Neeway et al. (2016)³⁶ and has a composition of
 196 $\text{K}_{1.3}\text{Mg}_{0.95}\text{Sn}_{2.1}\text{S}_6$ ⁴⁰. The sulfide component of the KMS-2 structure provides a reduction
 197 capacity of 21 000 $\mu\text{eq electrons/g}$ ³⁶ and produces a final Tc product of $\text{Tc(IV)}_2\text{S}_7$. With this high
 198 reduction capacity and ability to function as an excellent Tc getter under high alkaline
 199 conditions, 2.35 g of the KMS-2 was added, which is enough to theoretically reduce all of the
 200 Cr(VI) and 10 times the Tc content present in the LAW simulant.

201 Silver exchanged zeolite (Sigma Aldrich) was also added to all systems to act as an
 202 iodide getter, the results of which are not presented in this work.

203 2.2.2 Cast Stone Fabrication

204 The compositions for the Cast Stone samples in this study are provided in Table 3. The
 205 Cast Stone has a composition of 47 wt% blast furnace slag (BFS), 45 wt% fly ash (FA) and 8
 206 wt% ordinary Portland cement (OPC). The Cast Stone was fabricated with a free water to dry
 207 blend ratio of 0.55. The mass of getter added was subtracted from the mass of the required dry
 208 materials. The remaining mass was comprised of the 47:45:8 BFS:FA:OPC ratio and the BFS,
 209 FA and OPC combined thoroughly prior to fabrication.

210 Table 3 – Fabrication recipes for the Cast Stone samples used in this study.

Batch ID	Total Dry Ingredients (g)	LAW ⁽¹⁾ Simulant Required (g) ⁽²⁾	Tc Spike (ppm)	Blast Furnace Slag (g)	Fly Ash, (g)	OPC (g)	Mass of Tc Getter (g)	Mass of I getter (g)
CS- Control	1750.0	1307.9	16	822.5	787.5	140.0	n/a	n/a
CS-Sn-A	1750.0	1307.9	16	798.3	764.3	135.9	Sn-A 50.0	Ag-Z 8.75
CS- KMS-2	1750.0	1307.9	16	820.7	785.8	139.7	KMS-2- SS 2.35	Ag-Z 1.45
Long Term Cast Stone	1767.5	1302.7	56	822.5	787.5	140.0	Sn-A 8.75	Ag-Z 8.75

211
 212 The getter was added to the liquid LAW simulant and allowed to react before the addition
 213 of the dry Cast Stone ingredients. The Sn-A was allowed to react for 48 h and the KMS-2 was
 214 allowed to react for 24 h with the LAW simulant. The shorter reaction time for KMS-2 is

215 because, based on previous observations, Tc removal by the KMS-2 is faster than Sn-A³⁴.
216 Aliquots of the liquid LAW simulant were collected before and after getter addition to determine
217 the extent of Tc removal by the getters.

218 Following the getter treatment the LAW simulant was stirred thoroughly using an electric
219 mixing impeller to ensure that the getter material was well dispersed. The dry Cast Stone
220 components were then introduced slowly over a 5 min time span with continual mixing. The
221 impeller rotation rate was kept at a level to ensure that little to no vortex was created to limit air
222 introduction to the mix. From the initial time of dry component addition, the mixture was
223 allowed to stir for 15 min. The Cast Stone was then poured into cylindrical plastic molds (2”
224 diameter × 4” height) and vortexed to remove any entrapped air. The molds were capped with a
225 perforated lid, placed into a sealed bucket and allowed to cure for 28 d at 100 % relative
226 humidity. This fabrication produced three sample sets: 1) a control sample with no getters added
227 (CS-control), 2) the Sn-A containing Cast Stone (CS-Sn-A) and 3) the KMS-2 containing Cast
228 Stone (CS-KMS-2).

229 **2.3 EPA Method 1315 Leach Testing**

230 Full details of Method 1315 leach testing are provided by the EPA²³, and a summary is
231 given here. After curing, the monoliths were weighed and placed in a holder consisting of a
232 plastic top ring and a 2” diameter plastic pipe bottom held together with fishing line. This holder
233 design ensures no more than 2 % of the overall surface of the monolith was covered by the
234 holder. The monoliths were placed into 2 L plastic buckets containing VZPW at a 9 mL : 1 cm²
235 surface area ratio (~1700 mL VZPW). The buckets were capped but air was not removed from
236 the headspace (i.e., leaching occurred under atmospheric conditions and in the presence of
237 atmospheric O₂ and CO₂). At the conclusion of each leaching interval, the monoliths were
238 removed from the VZPW, weighed, photographed and then placed into other buckets filled with
239 the appropriate amount of fresh VZPW leachant. The leaching intervals were 2 h, 1 d, 2 d, 7 d,
240 14 d, 28 d, 42 d and 63 d. The leachates were analyzed with inductively coupled plasma mass
241 spectroscopy (ICP-MS) for Tc or inductively coupled plasma optical emission spectroscopy
242 (ICP-OES) for Cr and Na. Ion chromatography (IC) was utilized for anion measurements, e.g.,
243 NO₃⁻.

244 **2.4 Spectroscopy**

245 **2.4.1 X-ray diffraction (XRD)**

246 XRD was used to determine the mineralogical composition of the samples. Powdered
247 samples were loaded into zero-background holders and diffraction data were collected with a
248 Rigaku Miniflex II Bragg-Brentano diffractometer using Cu-K α radiation ($\lambda = 1.5418 \text{ \AA}$) and a
249 graphite post-diffraction monochromator. A known amount of rutile (TiO₂) standard was added
250 to each sample for quantitative analysis. Quantitative Rietveld refinements were carried out with
251 the Bruker TOPAS software (v4.2, Bruker AXS) using crystal structures for the relevant phases.

252

253 2.4.2 Single Particle Digital Autoradiography (iQid)

254 “Single-particle digital autoradiography”, with the ionizing-radiation Quantum Imaging
255 Detector (iQID)⁴², was used to assess the spatial distribution of ⁹⁹Tc within cross sectioned Cast
256 Stone “pucks”. The iQID imager comprises a scintillator (ZnS) in direct contact with a micro-
257 channel plate image intensifier and a lens for imaging the intensifier screen onto a charge
258 coupled device (CCD) or complementary metal oxide semiconductor (CMOS) camera sensor, all
259 within a compact light-tight enclosure. Individual photons or particles absorbed in a scintillator
260 crystal or phosphor screen produce a flash of light that is amplified via the image intensifier by a
261 factor of 10⁴ to 10⁶ and then imaged onto the camera. Scintillation flashes associated with
262 individual events are captured with high resolution with an array of pixels and referred to as an
263 event cluster. iQID’s ability to localize charged particles, both spatially and temporally, on an
264 event-by-event basis enables radionuclide distributions to be quantified at mBq-levels.
265 Autoradiographs are constructed in real time at high spatial resolution with an unrestricted
266 dynamic range. For the Cast Stone cross section imaging experiments, a 4-megapixel camera
267 (2048 × 2048 pixels) was used that acquires full-resolution images at approximately 10 frames
268 per second. Disks sectioned from within ~ 0.5” of the center of the Cast Stone monoliths were
269 analyzed using the iQID. The disks, which had a smooth surface, were placed on a scintillation
270 screen for collection times of 45 h. The effective physical size of each pixel during the image
271 acquisition was 55.8 μm with the final images displayed having an effective pixel size of 111.5
272 μm (2x2 binning). The pixel value corresponds to the number of beta particles detected at that
273 location during the 45 h image run. A test sample with small droplets of TcO₄⁻ enclosed in mylar
274 film was also analyzed to ensure the β-decay signal arises from specific sample areas, with a
275 strong correlation. Further information regarding development and use of the technique can be
276 found in Miller et al.⁴².

277 2.4.3 X-ray Absorption Spectroscopy (XAS)

278 Tc K-edge X-ray absorption spectroscopy (XAS) data were obtained at the Stanford
279 Synchrotron Radiation Lightsource Beamline 11-2. The monochromator was detuned 50% to
280 reduce the harmonic content of the beam. Transmission data was obtained using Ar-filled ion
281 chambers. Fluorescence data were obtained using a 100 element Ge detector and data were
282 corrected for detector dead time. Raw XAS data were converted to spectra using SixPack⁴³.
283 Spectra were normalized using Athena⁴⁴. Non-linear least squares fits of the normalized X-ray
284 absorption near edge spectroscopy (XANES) spectra were obtained using standard spectra and
285 the locally-written program, *fites* (<http://lise.lbl.gov/RSXAP>). XANES standard spectra were
286 carefully energy calibrated using TcO₄⁻ adsorbed on Reillex-HPQ as the energy reference. The
287 XANES spectral resolution is 7 eV based on the width of the TcO₄⁻ pre-edge peak. Sample
288 spectra were convolved with a 1.8 eV Gaussian to match the resolution of the TcO₄⁻ adsorbed on
289 Reillex-HPQ standard spectra. Six standard spectra (TcO₄⁻, Tc₂S₇, Tc(V)=O polyoxometallate,

290 Tc(IV) gluconate, $\text{TcO}_2 \cdot 2\text{H}_2\text{O}$ and a Tc(IV) EDTA complex) were used in the initial fitting of
291 the sample XANES spectra. Cast Stone samples were selected and ground with a mortar and
292 pestle to $< 300 \mu\text{m}$ particle size for XAS analyses.

293 *2.4.4 Micro X-ray Fluorescence Spectroscopy (μ -XRF)*

294 μ -XRF provides elemental distribution information within a sample. μ -XRF analysis was
295 performed on un-leached Cast Stone samples using an Orbis Micro-XRF Analyzer with a Mo X-
296 ray source and a silicon drift detector. Elemental data were collected under vacuum using a 45
297 kV polychromatic beam focused to $30 \mu\text{m}$ using a poly-capillary optic and displayed as number
298 of counts per element-specific energy levels. The Cast Stone samples used for μ -XRF were
299 chiseled from the Cast Stone pucks used in iQid imaging. The samples were mounted in epoxy
300 resin (Streuers) in a stainless steel ring. After mounting, the sample was sliced using a low speed
301 disc saw (Isomet) to a thickness of $\sim 100 \mu\text{m}$. The sample was then polished, water free, to a 0.1
302 μm diamond finish. The thin slide sample was then analyzed with iQid and μ -XRF.

303 **3. Results and Discussion**

304 *3.1 Tc Removal by Getters*

305 In order to limit diffusivity from the Cast Stone into the leachant, the Tc must first be
306 removed from the LAW simulant solution by the getters. Figure 1 a) shows the percentage of
307 initial Tc (16 ppm) removed from the LAW simulant by the getters. Sn-A added at a $50 \text{ g} : 1 \text{ L}$
308 ratio removed 65% of the Tc from solution, below the theoretical removal capacity. This is
309 within the range of removal previously observed at this ratio of Sn-A to Tc³⁵. The expected
310 product of the removal is $\text{Tc(IV)O}_2 \cdot x\text{H}_2\text{O}$. The KMS-2 removed 98 % of Tc from the LAW with
311 a ratio of only $2.35 \text{ g} : 1 \text{ L}$. The final product of the Tc removal from LAW has been identified
312 as a $\text{Tc(IV)}_2\text{S}_7$ species³⁶, comprised of two Tc centers connected through a sulfide linkage⁴⁵.
313 This minimal amount of KMS-2 added to achieve high levels of Tc removal highlights the
314 prospect of sulfide-bearing materials to be used for redox treatments under chemically extreme
315 conditions.

316 The results show that not all of the Tc(VII) initially in the LAW simulant was removed
317 by the getter, even though a sufficient mass of each getter was added to provide a reduction
318 capacity capable of complete Tc removal. One reason why not all of the Tc(VII) was removed is
319 that Cr(VI) in solution can hinder Tc(VII) removal by getter materials through competitive redox
320 processes. Cr(VI) has a higher standard reduction potential of 1.33 V compared with 0.78 V for
321 Tc(VII)O_4 ^{-46,47} and thus Cr(IV) is preferentially reduced. Figure 1 b) shows the % Cr removed
322 by the getters prior to fabricating the LAW simulant. The Sn-A removed $> 99\%$ of the initial Cr,
323 873 ppm, from the LAW simulant. Following contact with the Sn-A, the LAW simulant lost its
324 yellow color and became colorless, indicating reduction and subsequent removal of the Cr(VI).
325 This level of Cr removal by the Sn-A suggests that it could be utilized for the removal of Cr(VI)

326 and other competitive redox species, with subsequent addition of a second material to target any
327 remaining redox active species.

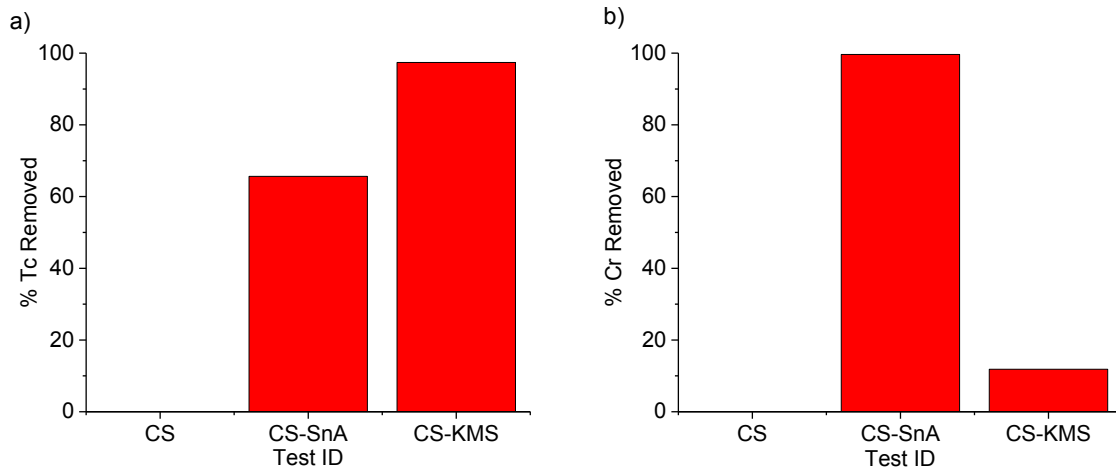


Figure 1 - the percentage of initial concentration of a) Tc (16 ppm) and b) Cr (873 ppm) removed from the LAW simulant by the Tc getters prior to Cast Stone fabrication.

328

329 On the other hand, KMS-2 only removed 12 % of the Cr from the LAW simulant. Given
330 the high reductive capacity of KMS-2, it is likely the Cr(VI) was reduced, in a similar way to the
331 case when Sn-A was used. Although, a color change in the LAW simulant from yellow to green-
332 blue after contact with the KMS-2 was observed, which suggests Cr(VI) reduction to Cr(III), it
333 appears that reduced Cr(III) was not removed from solutions and is likely present as a soluble
334 Cr(III) species. In both the Sn-A and KMS-2 cases, the amount of Tc getter added was based on:
335 (i) the reductive capacity of the material; and (ii) overcoming deleterious effects of pH and
336 competing redox reactions on getter performance. The results from our study demonstrated that
337 this approach led to highly successful Tc removal from the LAW simulant, and should be used in
338 future efforts of this and similar types.

339 **3.2 Leach Testing of Getter-Containing Cast Stone**

340 **3.2.1 Measurement of Observed Diffusivity**

341 Cementitious waste forms are comprised of a complex, porous structural matrix. As a
342 result, diffusion of species out of the matrix via physical processes is restricted⁴⁸. The chemical
343 reactivity of the cementitious waste form also adds additional restraints to diffusion of species
344 from the waste form to the contacting solution; more so in the presence of chemically reactive
345 getters. Therefore, the release of species from cementitious materials is best represented if both
346 chemical reactions and physical processes are considered^{49,50}. Although operationally defined,
347 the observed diffusivity (D_{obs}) incorporates the effects of both factors and is most suitable for

348 measurement and comparison of diffusion (i.e., release) rates of contaminants of interest from a
349 cementitious waste form.

350 Observed diffusivity is calculated for individual species using a solution for Fick's 2nd
351 law for simple radial diffusion into an infinite bath from a cylinder shape, similar to the one used
352 in Cast Stone leaching through EPA Method 1315. The effective diffusivity is calculated after
353 each leaching interval using Equation 1:

$$354 \quad D_{obs} = \pi \left[\frac{M_{t_i}}{2\rho C_o(\sqrt{t_i} - \sqrt{t_{i-1}})} \right]^2 \quad \text{Equation 1}$$

355

356 where D_{obs} = observed diffusivity of a specific constituent for leaching interval, i (m^2/s)

357 M_{t_i} = mass of specific constituent released during leaching interval (mg/m^2)

358 t_i = cumulative contact time at the end current leach interval, i (s)

359 t_{i-1} = cumulative contact time after previous leaching interval, $i-1$ (s)

360 C_o = initial concentration of constituent relative to the dry Cast Stone mass (mg/kg_{dry})
361 calculated using the theoretical initial constituent concentration in the simulant based on
362 additions made in simulant preparation.

363 ρ = Cast Stone dry bulk density (kg_{dry}/m^3).

364 The common units for observed diffusivity are cm^2/s and the output from equation 1
365 (m^2/s) is multiplied by 10 000 to convert to these units.

366 The D_{obs} term is also defined from the quotient of an intrinsic diffusivity (D_i) and a
367 chemical capacity factor (α). This relationship is shown in equation 2:

$$368 \quad D_{obs} = \frac{D_i}{\alpha} \quad \text{Equation 2}$$

369 The D_i term is representative of the physical influence impacting diffusion from the
370 cementitious material. The value of D_i depends on the tortuosity (τ), constrictivity (δ) and
371 porosity (ϵ) of complex cementitious structure. These factors adjust the diffusion coefficient of a
372 solute in dilute water (D_f) in equation 3.

$$373 \quad D_i = D_f \frac{\epsilon\delta}{\tau^2} \quad \text{Equation 3}$$

374 The tortuosity term is representative of the diffusing species traveling a longer distance
375 than assumed in a linear diffusion pathway due to the porous network within the cementitious
376 waste form. The constrictivity term depends on the ratio of the diameters of the smallest and

377 largest pores in the system. Both are dimensionless parameters and, along with porosity, are
378 dominantly used in models as empirical parameters to measure D_{obs} .

379 The chemical component, α , is utilized to combine a myriad of interactions between
380 species and the cementitious material including redox processes, ion exchange, sorption and
381 associated kinetics. Assuming fast and reversible chemical interactions and sorption processes
382 that follow a linear isotherm, α can be calculated as follows:

$$383 \quad \alpha = \varepsilon + \rho K_d \quad \text{Equation 4}$$

384 Where K_d is the distribution coefficient representing the ratio of the amount of a species
385 sorbed to a solid surface vs. the amount present in solution at equilibrium. For species that do
386 not interact with the waste form, such as Na^+ and NO_3^- , a K_d of zero would be expected and the
387 value of the chemical component α would depend solely on the porosity. Such species are
388 termed to be “mobile”. In the case of redox sensitive species, the K_d and the chemical
389 component α will be influenced by sorption and redox reactions, and a comparison between the
390 D_{obs} value measured for the redox sensitive species and a mobile constituent should be
391 performed to determine the effect of the additional chemical reactions on contaminant
392 diffusivity.

393 3.2.2 EPA Method 1315 Leach Testing

394 Following the 28 d curing procedure, the Cast Stone monolith samples were leached in
395 simulated Hanford VZPW using the conditions described in EPA Method 1315. VZPW
396 represents the likely disposal conditions experienced by a waste form in a shallow subsurface
397 disposal site, such as the IDF. The Tc D_{obs} over a 63 d leaching time for the three Cast Stone
398 systems is shown in Figure 2 a). The control monoliths without Tc getters added (CS-Control)
399 showed a continual increase in Tc D_{obs} before reaching a steady state at 42 d. After 63 d
400 leaching, the Tc D_{obs} for the CS-Control was $4.6 \pm 0.2 \times 10^{-12} \text{ cm}^2/\text{s}$. This value is within the
401 expected range of previous measurements of Cast Stone fabricated with simulated LAW⁵¹. In
402 the most recent *Tank Closure and Waste Management Environmental Impact Statement for the*
403 *Hanford Site, Richland, Washington*⁵², the Washington State Department of Ecology highlights
404 that lowering the diffusivity of a species to a performance standard of $1 \times 10^{-12} \text{ cm}^2/\text{s}$ at a
405 groundwater infiltration rate of 3.5 mm/y would “delete this waste (i.e. the waste form being
406 investigated) from the list of dominant contributors to risk”.

407 As the Tc getters act by reducing the Tc(VII)O_4^- to an sparingly soluble Tc(IV) species, a
408 chemical oxidation step is required in order for the Tc to be released. This is highlighted by
409 measurement of the D_{obs} for a “mobile constituent” which does not chemically interact with the
410 Cast Stone. Figure 2 b) displays the Na D_{obs} measured during the leaching period. It should be
411 noted that the baseline Na content (5 mmol/L) of the VZPW was subtracted in the calculation of
412 D_{obs} . For the CS-Control, the Na D_{obs} continually decreased from $1.7 \pm 0.6 \times 10^{-8} \text{ cm}^2/\text{s}$ at the 1
413 d interval to $3.9 \pm 0.1 \times 10^{-9} \text{ cm}^2/\text{s}$ at the 63 d interval. The Tc D_{obs} values are many orders of

414 magnitude lower than the “mobile” Na D_{obs} value, indicating that the mechanism of Tc release is
415 a slow chemical reaction involving re-oxidation of the Tc. In the CS-Control, a portion of the Tc
416 will be present in a reduced Tc(IV) state due to the reducing BFS component within the Cast
417 Stone⁴⁵.

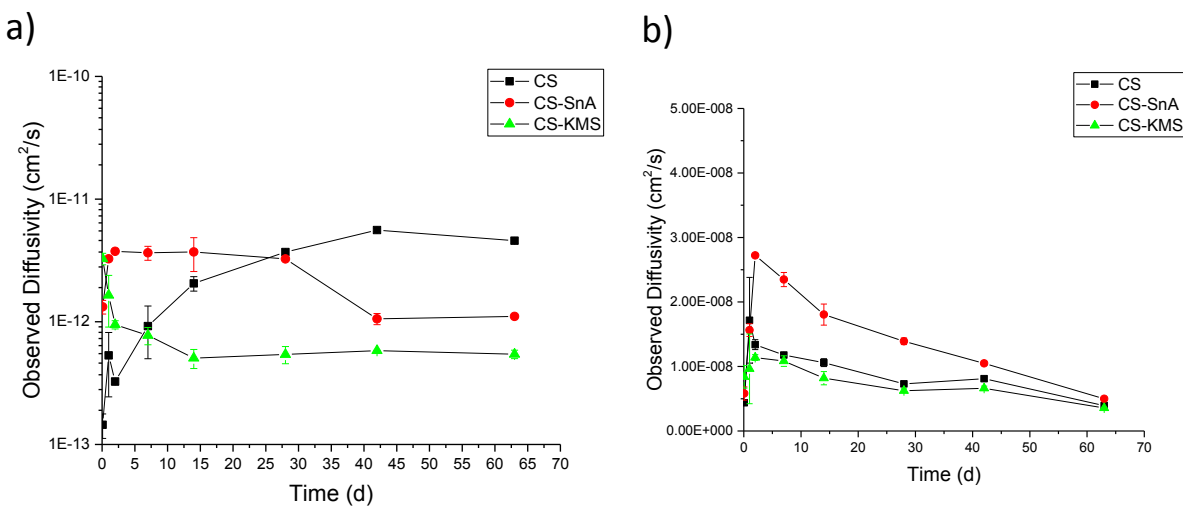


Figure 2 - a) the resulting Tc D_{obs} measured and b) the resulting Na D_{obs} values during the 63 d leaching period of the Cast Stone monoliths with and without Tc getters. The Cast Stone monoliths were leached in VZPW and placed into a fresh leachant at each interval at a sample surface area to leachate volume of 1 cm² : 9 mL. The errors bars represent the standard deviation of the mean on the two leaching samples.

418 The D_{obs} values measured for Tc leached from the Cast Stone samples containing Sn-A
419 (CS-Sn-A) during the first 28 d interval are higher or equal to the CS-Control (Figure 2a). After
420 28 d, the Tc D_{obs} values decreased to $1.1 \pm 0.01 \times 10^{-12}$ cm²/s at 63 d. In longer leaching times,
421 the presence of the Sn-A getter improved the retention of Tc. It is possible that the Sn-A may
422 have increased the release of species from the Cast Stone monolith. In the Na D_{obs} , (Figure 2 b),
423 the CS-Sn-A also had the highest measured values in the initial stages of leaching reaching a
424 maximum of $2.7 \pm 0.002 \times 10^{-8}$ cm²/s at the 2-d interval. As no interactions occur between Na
425 and the Cast Stone, this increase must arise from the physical properties of the monolith, as
426 described previously. The CS-Sn-A included 50 g of Sn-A added in the Cast Stone, and this
427 large addition of material may have distorted the structure, leading to larger pore sizes and
428 allowing for more rapid diffusion of species. This highlights the need to consider physical
429 impacts resulting from addition of getters to cementitious materials.

430 The KMS-2 was highly successful in sequestering Tc from the LAW simulant prior to
431 fabrication of the Cast Stone. By removing > 98 % of the Tc from solution, this system provided
432 the greatest Tc retention in the Cast Stone. The Tc D_{obs} values measured for the KMS-2
433 containing Cast Stone (CS-KMS-2) in Figure 2 a) support this hypothesis. The Tc D_{obs} for the
434 CS-KMS-2 monolith after 2 d were below the D_{obs} for the CS-Control, with little change over

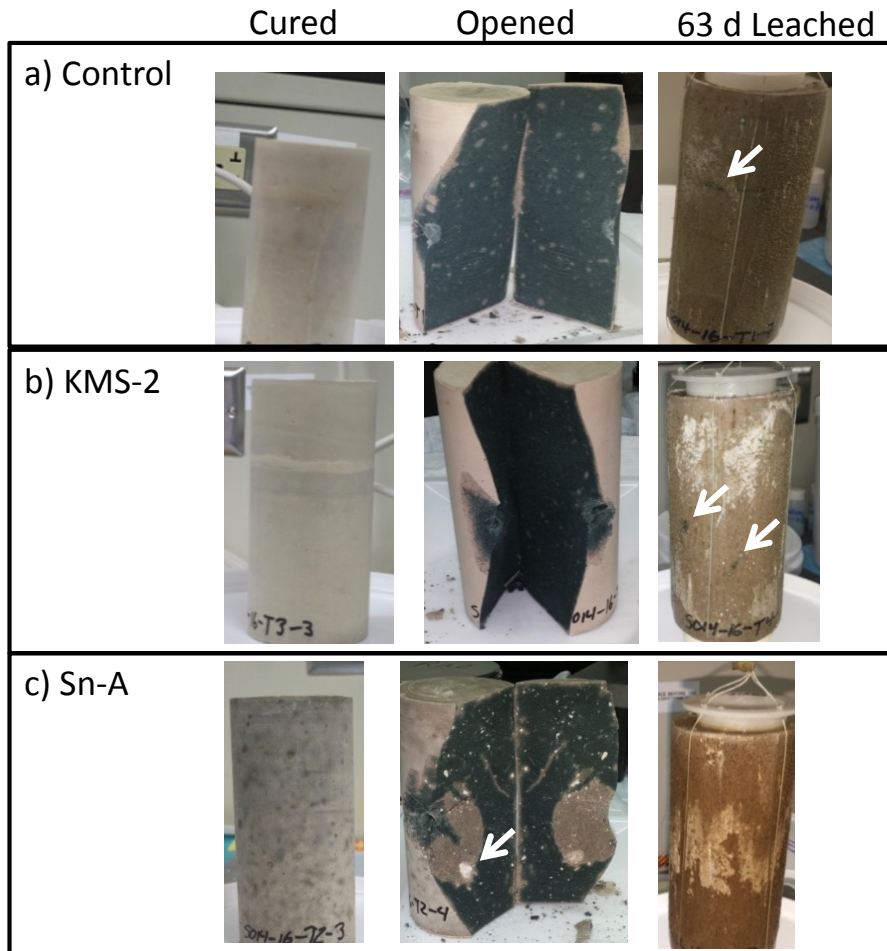
435 time. At 63 d, the Tc D_{obs} was $5.4 \pm 0.4 \times 10^{-13} \text{ cm}^2/\text{s}$, a near order-of-magnitude improvement
436 over the CS-Control. This substantial improvement was achieved with only a minor addition of
437 KMS-2, equivalent to $< 0.01 \text{ wt}\%$ of the overall mass of the waste form. KMS-2 as a Tc getter is
438 highly effective in removing Tc from extreme chemical environments and controlling Tc release
439 from the subsequently fabricated Cast Stone waste form. The Na D_{obs} for the CS-KMS-2 system
440 was similar to the CS-Control ($3.6 \pm 0.7 \times 10^9 \text{ cm}^2/\text{s}$ at 63 d leaching). Further studies to
441 determine the ideal KMS-2 getter loading amount and investigate the performance of other
442 sulfide-containing materials as Tc getters are ongoing.

443 ***3.3 Characterization of Tc Getter Containing Cast Stone***

444 *3.3.1 Cast Stone Characteristics*

445 Solid-phase characterization of the monolith samples provides information on the
446 mechanism of Tc location and retention in the Cast Stone. Although the Cast Stone samples are
447 relatively similar in mineralogical composition throughout, see Supplemental Information Table
448 S1, visible differences exist between the Cast Stone samples, as shown in the photographs Figure
449 3. Following curing, the interior and exterior of the CS-Control and the CS-KMS-2 look
450 identical, Figures 3 a) and c), respectively. Both samples display a dark blue-green interior as a
451 result of the presence of sulfur based radicals from the blast furnace slag. As is typical of blast
452 furnace slag based cement, the dark blue color fades to gray upon oxidation. However, after 63 d
453 leaching in VZPW, two primary features developed on the exterior of the CS-Control and CS-
454 KMS-2. First, a white film forms on the monolith wall, beginning at the 1 d interval. This white
455 deposit was identified by XRD as aragonite (a CaCO_3 polymorph). Growth of this film may
456 contribute to the slowed release of species from the Cast Stone to solution over long exposure
457 timeframes by providing a physical barrier to diffusion. However, after 63 d leaching, this film is
458 not uniform, nor complete. Dark regions, denoted by white arrows in Figures 3 a) and b), also
459 developed during the leaching period and these regions were further investigated using scanning
460 electron microscopy. Tc was only identified within this dark region and not outside of it (see
461 Figure S1 in the supplemental information).

462 The CS-Sn-A (Figure 3 c) displayed increased heterogeneity compared with the CS-
463 Control. A blotchy pattern can be seen on the exterior of the monolith, likely a result of the
464 higher loading of the getter added to the Cast Stone. Another observation was made upon
465 opening the monolith: the dark blue-green color was present in the interior regions of the
466 monoliths and two additional features were also prominent. These are white, isolated regions
467 (marked with an arrow in the figure), which are surrounded by a region of brown coloration.
468 Samples from both white and brown areas were collected and analyzed by XRD. The white
469 areas were primarily comprised of burtite ($\text{CaSn}(\text{OH})_6$) and cassiterite (SnO_2), and are both
470 remnants of the added Sn-A. The brown region surrounding the white areas was similar to the
471 bulk Cast Stone (i.e., highly amorphous), but also contained burtite. This heterogeneity confirms
472 that the distribution of getters within the Cast Stone matrix is uneven.



473

474 Figure 3 - photographs of the Cast Stone monoliths in their cured form, opened after curing and
 475 following 63 d leaching for a) the control system with no getters, b) Sn-A containing Cast Stone
 476 and c) KMS-2 containing Cast Stone

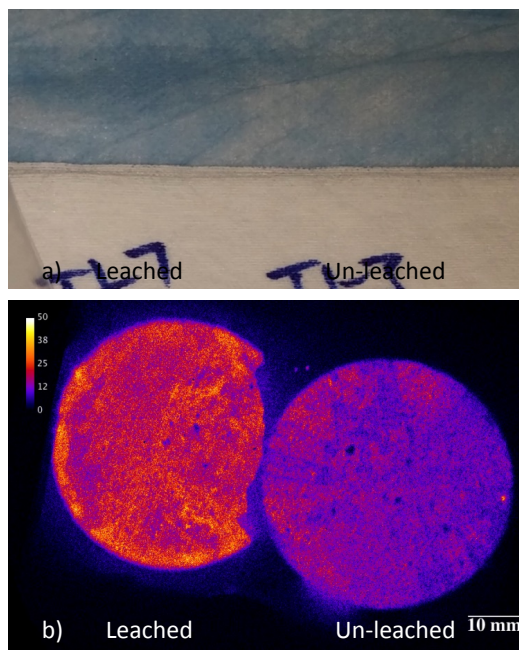
477 *3.3.2 Tc Distribution in Cast Stone*

478 To develop an understanding of Tc behavior in Cast Stone, the Tc must be located within
 479 the sample and the chemical composition of these locations characterized. With the low overall
 480 concentration of Tc in the leached samples (16 ppm in the LAW simulant, or 5 μg Tc/kg of wet
 481 Cast Stone), Tc cannot be detected through the use of many conventional spectroscopic
 482 techniques. However, Tc does possess a unique signature in its β -decay which can be utilized to
 483 map its distribution within the Cast Stone.

484 Traditional contact radiography has been previously utilized to image Cs and Sr
 485 distribution in cementitious materials⁵³. The drawback of this technique is it is an “all in”
 486 measurement in that the analyst must wait until the end of the measurement to observe if a useful
 487 image has been produced on the radiography film and the experiment cannot be tuned for
 488 varying types of radiation and intensity. However, the single particle digital autoradiography

489 technique (iQid), employed to analyze the Cast Stone samples in our study, is much more
490 advantageous because it provides real-time imaging of individual radioactive decay events and is
491 tunable to specific forms of radiation.

492 In the presented iQid images (Figure 4-9), the color scale for the images represents the
493 relative number of β -decays measured at that individual pixel. Each pixel has a resolution of ~ 10
494 μm . . . Brian confirm. The brighter the signal in the image corresponds to a higher number of
495 detected β -decays, and therefore a higher concentration of Tc, at that location. All images are
496 presented with identical collection settings. An example of Tc detection and detection efficiency
497 is shown in the Supplemental Information Figure S2.

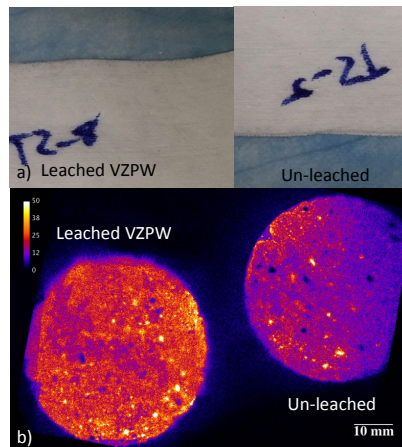


498

Figure 4 - a) photographs of the cross-sectioned pucks from the CS-Control monolith after 63 d leaching in VZPW and before leaching and b) the corresponding iQid images showing Tc distribution.

499 A cross section or “puck” was cut from the center of the Cast Stone samples before and
500 after 63 d leaching. Figure 4 displays the iQid images collected from the CS-Control with the
501 63-d leached puck on the left side of the image. Photographs of the pucks are also presented for
502 reference, the dark green interior observed in Figure 3 is not present on the puck surface due to
503 air oxidation at the time of the photograph of the puck. In the iQid image of the unleached CS-
504 Control, the β -decay signal is relatively evenly distributed throughout the sample. In the 63-d
505 leached sample, the Tc remains distributed evenly in the sample although a stronger Tc signal
506 arises from regions near the outer edge (between the 5 and 10 o’clock positions). This increased
507 signal on the outer edge may be indication of a physical barrier to Tc transport from the outer
508 wall carbonate deposit This distribution of Tc in the getter-free system demonstrates thorough

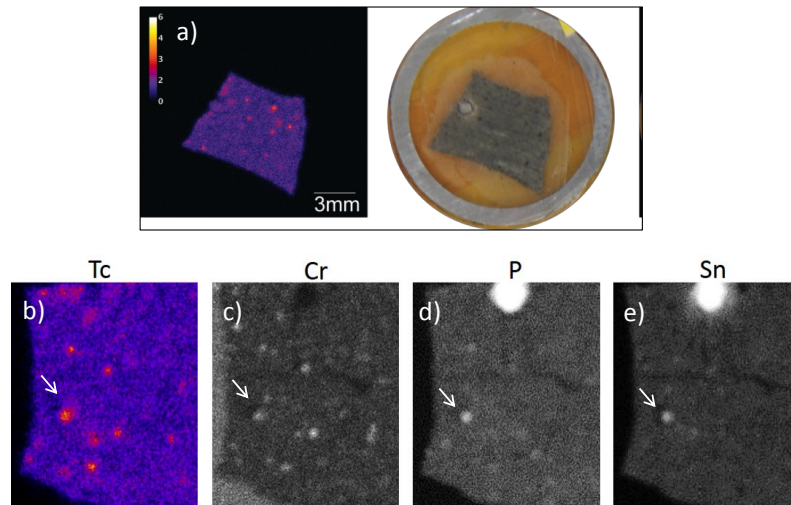
509 mixing during Cast Stone fabrication, ensuring a homogenous composition. Environmental
510 modelling of release from waste forms also assumes a homogenous source. The brighter image
511 in the 63-d leached sample may be due to the leaching process, and a combination of factors
512 including the effect of water penetration into the monolith and the impact this has on both the
513 porosity of the Cast Stone matrix and the Tc distribution. An increase in porosity would allow
514 increased β decay events to reach the detector without being masked by a solid interface, thus the
515 signal will appear stronger, even if the Tc concentration is similar, as a result of the increase in
516 effective sampling volume of the iQid detector. This inhibits the ability to quantitatively compare
517 images from one sample to another.



518
519 Figure 5 - a) photographs of the cross-sectioned pucks from the CS-Sn-A monolith after 63 d
520 leaching in VZPW and before leaching and b) the corresponding iQid images showing Tc
521 distribution.

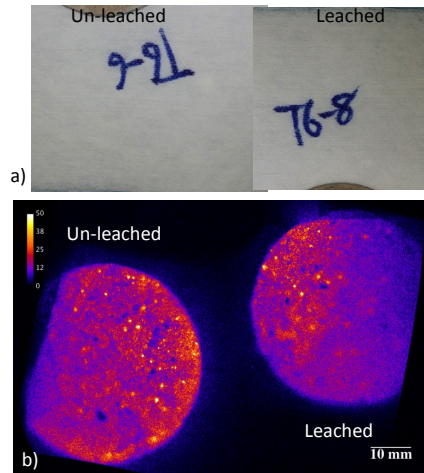
522
523 The introduction of Tc getters to the Cast Stone has a large effect on Tc distribution
524 within the sample. Figure 5 displays the iQid images collected from the CS-Sn-A pucks. In the
525 un-leached sample, distinct regions of higher signal, or “hot spots”, are present throughout the
526 sample corresponding to higher levels of Tc. Following leaching, the hot spots are still present
527 with some congregating near the outer edge. A sample of the hot spot region was extracted from
528 an un-leached Sn-A Cast Stone monolith for further analysis. This sample was mounted in epoxy
529 and imaged with the iQid, Figure 6 a). In the iQid image, several hot spots were observed. This
530 activity map can then be correlated with additional elemental mapping using μ -XRF. One hot
531 spot is highlighted by an arrow in the iQid image in Figure 6 b). This location also has an
532 accumulation of Cr, a redox active constituent like Tc, as shown in the μ -XRF map in Figure 6
533 c). There are also prominent signals from P and Sn at this location in Figures 6 d) and e), arising
534 from the residual Sn-A. This correlation between the position of the Tc, Cr, Sn and P
535 demonstrates that redox-active species (Cr and Tc) removed from the LAW simulant by the Sn-
536 A getter remain associated with the Sn-A getter in the Cast Stone matrix. At the top of the XRF
537 map in Figure 6 d) and e), a large signal from P and Sn is present. This signal corresponds to the
538 white area on the left edge of the sample in Figure 6 a). From the iQid image in Figure 6 b),

539 there was no Tc signal associated with this area, but there is a Tc signal coming from the area
540 surrounding the white area, suggesting that Tc reacted with the surface of the getter and was not
541 incorporated into the Sn-A structure.
542

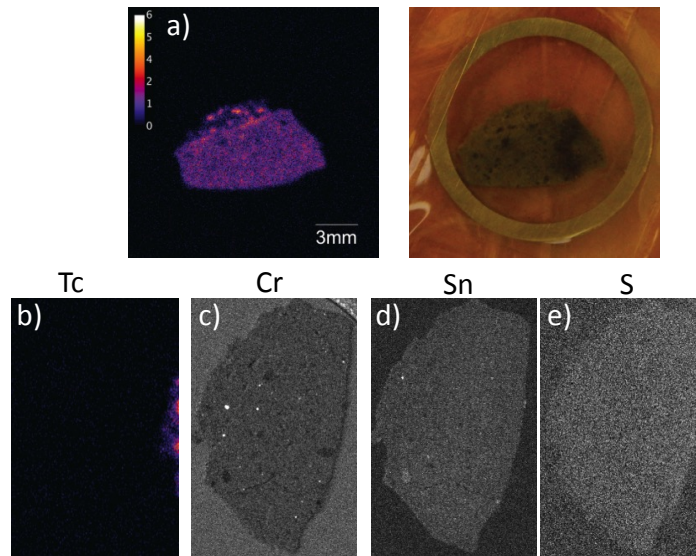


543 Figure 6 - a) iQid image and photograph of the sample extracted from the CS-Sn-A, b) magnified
544 iQid image showing several Tc hot spots and the corresponding μ -XRF maps of c) Cr, d) P and
545 e) Sn. The white arrow in b) – e) highlights the same spot in each image.

546 After identifying Tc “hot spots” in the vicinity of the Sn-A added as Tc getter within the
547 Cast Stone matrix, pucks from the monoliths of CS-KMS-2 were also analyzed with the iQid
548 (Figure 7). Tc hot spots are visible in the iQid image of the unleached KMS-2 Cast Stone and
549 the hot spots remain even after leaching. Due to the smaller particle size and low amount of
550 KMS-2 added, correlating the Tc hot spots to KMS-2 rich locations within Cast Stone matrix is
551 challenging, given the 30 μ m resolution of the μ -XRF. A slice of the unleached KMS-2 Cast
552 Stone was imaged with the iQid (Figure 8 a) and b). The corresponding elemental maps show
553 some Cr isolations in the sample (Figure 8 c). Sn and S are the two largest components of the
554 KMS-2 yet their XRF maps do not correlate to the Tc hot spots (Figures 8 d) and e). However, it
555 is likely that the Tc is associated with the KMS-2 getter in the CS-KMS-2 based on
556 circumstantial evidence. For example, Tc(VII) was entirely removed from the LAW simulant
557 after KMS-2 addition, the Tc hot spots were only observed in the getter containing Cast Stone
558 samples, and in the CS-Sn-A there is clear evidence that the Tc associated with the getter.
559
560



561
 562 Figure 7 a) photographs of the cross-sectioned pucks from the CS-KMS-2 monolith after 63 d
 563 leaching in VZPW and before leaching and b) the corresponding iQid images showing Tc
 564 distribution.



565
 566 Figure 8 - a) iQid image and photograph of the sample extracted from the CS-KMS-2, b)
 567 magnified iQid image showing several Tc hot spots and the corresponding μ -XRF maps of c) Cr,
 568 d) Sn and e) S.

569 3.3.3 Influence of Tc oxidation state within Cast Stone

570
 571 By remaining associated with the getters in the Cast Stone, the sequestered Tc will likely
 572 remain in the chemical state generated upon reaction with the getter. Sn-A has been shown to
 573 sequester Tc as a hydrated Tc-oxide, $\text{Tc(IV)O}_2 \cdot x \text{H}_2\text{O}$ ³⁵, while the KMS-2 generates a Tc-
 574 sulfide, $\text{Tc(IV)}_2\text{S}_7$ ³⁶.

575

576 This difference in final Tc solid product could result in the differences in D_{obs} during
577 leaching of the two Cast Stone systems. Analysis of a long-term (6 month) leached Cast Stone
578 sample provides additional information the effect that Tc speciation has on Tc retention in the
579 Cast Stone. Cast Stone samples were fabricated using a higher Tc spike of 56 ppm in the LAW,
580 thus allowing Tc K-edge XANES analysis to determine oxidation state and local environment;
581 however the Cast Stone composition remains unchanged. Results from the XAS analyses for the
582 Cast Stone before and after 6 months leaching in VZPW are presented in Figure 9. Linear
583 combination fitting of the XANES for the unleached sample (Figure 9 A) gave a Tc speciation of
584 59 % $Tc(VII)O_4^-$, 13 % of $Tc(IV)_2S_7$ and 28 % $Tc(IV)O_2$. After 6 months leaching (Figure 9 b),
585 the Tc in the Cast Stone sample was composed of 76 % $Tc(VII)O_4^-$, 11 % of $Tc(IV)_2S_7$ and 13 %
586 $Tc(IV)O_2$. The primary difference between the two samples was the increase in the $Tc(VII)O_4^-$
587 component and the decrease in $Tc(IV)O_2$ component for the 6 month leached sample, while the
588 amount of $Tc(IV)_2S_7$ remained largely unchanged. This result shows that during the 6 month
589 leaching period, the TcO_2 is preferentially re-oxidized to TcO_4^- and that the Tc_2S_7 is more
590 resistant to re-oxidation to mobile TcO_4^- . Previous analysis of cementitious based systems have
591 revealed that BFS and the addition of FeS and NaS provided increased reduction of $Tc(VII)$
592 within the waste form⁵⁴. As the KMS-2 sequestered > 98% of the Tc from the LAW as Tc_2S_7 ,
593 this Tc species will be more resistant to re-oxidation, thus slower to convert to mobile TcO_4^-
594 leading to the improvement in diffusivity which was observed in the leach testing. Previous
595 analysis of cementitious based systems have revealed that BFS and the addition of FeS and NaS
596 provided increased reduction of $Tc(VII)$ within the waste form.

597
598 Previous Tc getter inclusion in cementitious waste forms (67 % OPC and 33 % BFS)
599 fabricated with a neutral simulated groundwater with lower Cr content and lower Tc spike (0.70
600 ppm) showed that both Sn-A and purolite resins were able to decrease Tc diffusivity⁵⁵. In this
601 work, we have demonstrated for the first time that a significant improvement in Tc retention and
602 diffusivity is possible when minimal amounts of a Tc getter, e.g., KMS-2, are used to remove Tc
603 from chemically extreme waste liquids with high pH, high ionic strength and in the presence of
604 substantial amounts of competing redox sensitive elements, such as Cr. By selecting getters
605 capable of sequestering Tc from the LAW environment, and by generating a more stable form
606 towards re-oxidation of Tc, (e.g., Tc_2S_7), it is possible to retain the Tc with the getter in the
607 cementitious waste form and decrease Tc leachability.

608

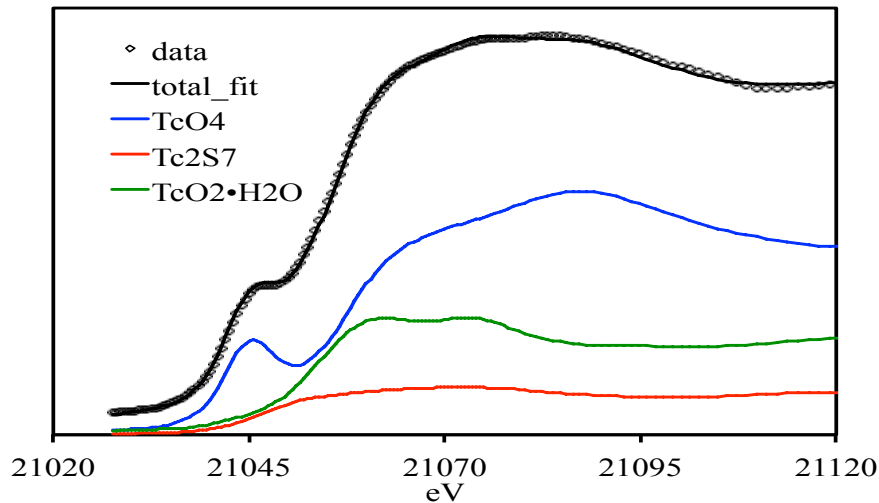


Figure 9 - Tc K-edge XANES spectrum and fit for the Cast Stone a) prior to leaching and b) after 6 month leaching in VZPW. The corresponding table shows the Tc K-edge fitting results for the Cast Stone samples analyzed. The numbers in parentheses represent the standard deviations of the contribution of that component for the ending digit, p is the probability that improvement of the fit, when this standard is included, is due to random error.

609 4.0 Conclusions

610 Two getter materials (Sn-A and KMS-2) were used in a pre-treatment contact step to remove Tc
 611 from simulated LAW prior to fabricating Cast Stone. The two getters were selected as each
 612 produced a different Tc final product: Tc(IV)-oxide via the Sn-A and Tc(IV)-sulfide via the
 613 KMS-2. Through a small addition of KMS-2 as a Tc getter (< 0.01 wt% of the total Cast Stone
 614 mass), > 98 % of the Tc was sequestered from the LAW. A higher addition of Sn-A was required
 615 to sequester 65 % of the Tc from the LAW. The sequestered Tc in the getter containing Cast
 616 Stone was identified to be primarily present as “hot spots” where it remained associated with the
 617 getter. The association of the Tc with the getters in the Cast Stone increased Tc retention in the
 618 solid and led to a significant reduction in the D_{obs} of Tc. The KMS-2 containing Cast Stone
 619 resulted in the largest decrease in Tc D_{obs} compared with Cast Stone without getters. Based on
 620 the results of this work, getters are a promising method to decrease contaminant release rates
 621 from cementitious waste forms fabricated with chemically extreme waste stream with minimal
 622 KMS-2 getter material addition.

623 Acknowledgements

624 Support for this project came from Washington River Protection Solutions. The authors
 625 wish to acknowledge the Kanatzidis group at Northwestern University for providing the KMS-2,
 626 RJ Lee Group (Richland, WA) for providing the Sn-Apatite, and Dave Swanberg (Washington
 627 River Protection Solutions, Supplemental Treatment Waste Form Development Project) for
 628 programmatic guidance, direction, and support. The authors acknowledge Ian Leavy, Erin
 629 McElroy, Steven Baum and Keith Geiszler for analyzing simulants and Cast Stone leachates.

630 SEM/EDS imaging was performed by Edgar Buck of PNNL. Tc K-edge XANES spectra were
631 obtained at the Stanford Synchrotron Radiation Lightsource, SLAC National Accelerator
632 Laboratory, which is supported by the U.S. Department of Energy, Office of Science, Office of
633 Basic Energy Sciences under Contract No. DE-AC02-76SF00515. Cr L-edge XAS data were
634 collected at the Advanced Light Source (ALS), Berkeley, which is supported by the Director,
635 Office of Science, Office of Basic Energy Sciences (OBES) of the U.S. Department of Energy
636 (DOE) under contract No. DE-AC02-05CH11231. A portion of this work (WWL) was supported
637 by the U.S. Department of Energy, Office of Science, Basic Energy Sciences, Chemical
638 Sciences, Biosciences, and Geosciences Division, Heavy Element Chemistry Program and was
639 performed at Lawrence Berkeley National Laboratory under contract No. DE-AC02-
640 05CH11231. The authors would like to thank Ben Williams for his expertise and assistance in
641 Cast Stone monolith fabrication.

642

643

- 645 (1) Jones, L.; WM Symposia, 1628 E. Southern Avenue, Suite 9-332, Tempe, AZ
646 85282 (United States): 2013.
- 647 (2) Ojovan, M. I.; Lee, W. E. *Metallurgical and Materials Transactions A* **2011**, *42*,
648 837.
- 649 (3) Gin, S.; Abdelouas, A.; Criscenti, L. J.; Ebert, W. L.; Ferrand, K.; Geisler, T.;
650 Harrison, M. T.; Inagaki, Y.; Mitsui, S.; Mueller, K. T.; Marra, J. C.; Pantano, C. G.; Pierce, E.
651 M.; Ryan, J. V.; Schofield, J. M.; Steefel, C. I.; Vienna, J. D. *Materials Today* **2013**, *16*, 243.
- 652 (4) Kruger, A. A.; Kim, D. S. *Proceedings of WM2015* **2015**, 1167469, Medium: ED.
- 653 (5) Polyakov, A. S.; Borisov, G. B.; Moiseenko, N. I.; Osnovin, V. I.; Dzekun, E. G.;
654 Medvedev, G. M.; Bel'tyukov, V. A.; Dubkov, S. A.; Filippov, S. N. *At Energy* **1994**, *76*, 181.
- 655 (6) Gephart, R. E. *Physics and Chemistry of the Earth, Parts A/B/C* **2010**, *35*, 298.
- 656 (7) Xu, K.; Hrma, P.; Rice, J. A.; Schweiger, M. J.; Riley, B. J.; Overman, N. R.;
657 Kruger, A. A. *Journal of the American Ceramic Society* **2016**, *99*, 2964.
- 658 (8) Zachara, J. M.; Serne, J.; Freshley, M.; Mann, F.; Anderson, F.; Wood, M.; Jones,
659 T.; Myers, D. *Vadose Zone Journal* **2007**, *6*, 985.
- 660 (9) Harrington, S.; Sams, T. *Proceedings of Waste Management Symposium* **2014**,
661 2014.
- 662 (10) Lenell, B. A.; Arai, Y. *Journal of Hazardous Materials* **2017**, *321*, 335.
- 663 (11) Langton, C. A. *Materials Research Society Symposium Proceedings* **1988**, *112*,
664 61.
- 665 (12) Faucon, P.; Adenot, F.; Jacquinet, J. F.; Petit, J. C.; Cabrillac, R.; Jorda, M.
666 *Cement and Concrete Research* **1998**, *28*, 847.
- 667 (13) Babaahmadi, A.; Tang, L.; Abbas, Z.; Zack, T.; Mårtensson, P. *Materials and*
668 *Structures* **2016**, *49*, 705.
- 669 (14) Swift, P.; Kinoshita, H.; Collier, N. C.; Utton, C. A. *Advances in Applied*
670 *Ceramics* **2013**, *112*, 1.
- 671 (15) Bird, G. W.; Lopata, V. J. In *Scientific Basis for Nuclear Waste Management*;
672 Northrup, C. J. M., Ed.; Springer US: Boston, MA, 1980, p 419.
- 673 (16) Palmer, D. A.; Meyer, R. E. *Journal of Inorganic and Nuclear Chemistry* **1981**,
674 *43*, 2979.
- 675 (17) Szecsody, J. E.; Jansik, D. P.; McKinley, J. P.; Hess, N. J. *Journal of*
676 *Environmental Radioactivity* **2014**, *135*, 147.
- 677 (18) Icenhower, J. P.; Qafoku, N. P.; Zachara, J. M.; Martin, W. J. *American Journal*
678 *of Science* **2010**, *310*, 721.
- 679 (19) Oostrom, M.; Truex, M. J.; Last, G. V.; Strickland, C. E.; Tartakovsky, G. D.
680 *Journal of Contaminant Hydrology* **2016**, *189*, 27.
- 681 (20) Westsik, J. H.; Piepel, G. F.; Lindberg, M. J.; Heasler, P. G.; Mercier, T. M.;
682 Russel, R. L.; Cozzi, A. D.; Daniel, W. E.; Eibling, R. E.; Hansen, E. K.; Reigal, M. R.;
683 Swanberg, D. J. *PNNL-22747, SRNL-STI-2013-00465* **2013**, Rev. 0, *Pacific Northwest National*
684 *Laboratory, Richland, Washington and Savannah River National Laboratory, Aiken, South*
685 *Carolina*.
- 686 (21) Westsik Jr, J.; Cantrell, K. J.; Serne, R. J.; Qafoku, N. *PNNL-23329, EMSP-RPT-*
687 *023* **2014**, *Pacific Northwest National Laboratory, Richland, WA*.
- 688 (22) Chung, C.-W.; Um, W.; Valenta, M. M.; Sundaram, S. K.; Chun, J.; Parker, K. E.;
689 Kimura, M. L.; Westsik Jr, J. H. *Journal of Nuclear Materials* **2012**, *420*, 164.

690 (23) EPA Method 1315 **2013**, US Environmental Protection Agency, Washington, DC.
691 (24) Mattigod, S. V.; Fryxell, G.; Parker, K.; Kaplan, D. In *MRS Proceedings*;
692 Cambridge Univ Press: 2002; Vol. 757, p II8. 7.
693 (25) Koivula, R.; Harjula, R. *Separation Science and Technology* **2010**, *46*, 315.
694 (26) Darab, J. G.; Amonette, A. B.; Burke, D. S. D.; Orr, R. D.; Ponder, S. M.;
695 Schrick, B.; Mallouk, T. E.; Lukens, W. W.; Caulder, D. L.; Shuh, D. K. *Chemistry of Materials*
696 **2007**, *19*, 5703.
697 (27) Wellman, D. M.; Mattigod, S. V.; Parker, K. E.; Heald, S. M.; Wang, C.; Fryxell,
698 G. E. *Inorganic Chemistry* **2006**, *45*, 2382.
699 (28) Li, D.; Kaplan, D. I.; Knox, A. S.; Crapse, K. P.; Diprete, D. P. *Journal of*
700 *Environmental Radioactivity* **2014**, *136*, 56.
701 (29) Levitskaia, T. G.; Chatterjee, S.; Pence, N. K.; Romero, J.; Varga, T.; Engelhard,
702 M. H.; Du, Y.; Kovarik, L.; Arey, B. W.; Bowden, M. E.; Walter, E. D. *Environmental Science:*
703 *Nano* **2016**.
704 (30) Sarri, S.; Misaelides, P.; Zamboulis, D.; Gaona, X.; Altmaier, M.; Geckeis, H. *J*
705 *Radioanal Nucl Chem* **2016**, *307*, 681.
706 (31) Long, K. M.; Goff, G. S.; Ware, S. D.; Jarvinen, G. D.; Runde, W. H. *Industrial*
707 *& Engineering Chemistry Research* **2012**, *51*, 10445.
708 (32) Qafoku, N.; Neeway, J. J.; Lawter, A. R.; Levitskaia, T. G.; Serne, R. J.; Westsik,
709 J., J.H.; Valenta Snyder, M. M. *PNNL-23282* **2014**, *Pacific Northwest National Laboratory*.
710 (33) Neeway, J. J.; Qafoku, N.; Serne, R. J.; Lawter, A. J.; Stephenson, J. R.; Lukens,
711 W. W.; Westsik Jr., J. H. *PNNL-23667* **2015**, *Pacific Northwest National Laboratory, Richland,*
712 *Washington*.
713 (34) Neeway, J. J.; Lawter, A. R.; Serne, R. J.; Asmussen, R. M.; Qafoku, N. P. In
714 *MRS Proceedings*; Cambridge Univ Press: 2015; Vol. 1744, p mrsf14.
715 (35) Asmussen, R. M.; Neeway, J. J.; Lawter, A. R.; Levitskaia, T. G.; Lukens, W. W.;
716 Qafoku, N. *Journal Of Nuclear Materials* **2016**, *480*, 393.
717 (36) Neeway, J. J.; Asmussen, R. M.; Lawter, A. R.; Bowden, M. E.; Lukens, W. W.;
718 Sarma, D.; Riley, B. J.; Kanatzidis, M. G.; Qafoku, N. P. *Chemistry of Materials* **2016**, *28*, 3976.
719 (37) Certa, P. J.; Empey, P. A. *ORP-11242* **2011**, *Revision 6, Washington River*
720 *Protection Solutions, LLC, Richland, Washington*.
721 (38) Brown, C. F.; Serne, R. J.; Bjornstad, B. N.; Horton, D. G.; Lanigan, D. C.;
722 Clayton, R. E.; Valenta, M. M.; Vickerman, T. S.; Kutnyakov, I. V.; Geiszler, K. N. *PNNL-*
723 *15503, Rev. 1* **2006**, *Pacific Northwest National Laboratory (PNNL), Richland, WA (US)*.
724 (39) Um, W.; Yang, J.-S.; Serne, R. J.; Westsik, J. H. *Journal of Nuclear Materials*
725 **2015**, *467, Part 1*, 251.
726 (40) Hassanzadeh Fard, Z.; Malliakas, C. D.; Mertz, J. L.; Kanatzidis, M. G. *Chemistry*
727 *of Materials* **2015**, *27*, 1925.
728 (41) Mertz, J. L.; Fard, Z. H.; Malliakas, C. D.; Manos, M. J.; Kanatzidis, M. G.
729 *Chemistry of Materials* **2013**, *25*, 2116.
730 (42) Miller, B. W.; Frost, S. H.; Frayo, S. L.; Kenoyer, A. L.; Santos, E.; Jones, J. C.;
731 Green, D. J.; Hamlin, D. K.; Wilbur, D. S.; Fisher, D. R. *Medical physics* **2015**, *42*, 4094.
732 (43) Webb, S. M. *Physica Scripta* **2005**, *2005*, 1011.
733 (44) Ravel, B.; Newville, M. *Physica Scripta* **2005**, *2005*, 1007.
734 (45) Lukens, W. W.; Bucher, J. J.; Shuh, D. K.; Edelstein, N. M. *Environmental*
735 *Science & Technology* **2005**, *39*, 8064.

- 736 (46) Haynes, W. M. *CRC handbook of chemistry and physics*; CRC press, 2014.
737 (47) Cobble, J. W.; Smith, W. T.; Boyd, G. E. *Journal of the American Chemical*
738 *Society* **1953**, *75*, 5777.
739 (48) van Brakel, J.; Heertjes, P. M. *International Journal of Heat and Mass Transfer*
740 **1974**, *17*, 1093.
741 (49) Atkinson, A.; Nelson, K.; Valentine, T. M. *Nuclear and Chemical Waste*
742 *Management* **1986**, *6*, 241.
743 (50) Atkinson, A.; Nickerson, A. K. *Nuclear Technology* **1988**, *81*, 100.
744 (51) Cantrell, K. J.; Westsik Jr, J. H.; Serne, R. J.; Um, W.; Cozzi, A. D. *PNNL-25194*
745 **2016**, *Pacific Northwest National Laboratory, Richland, WA*.
746 (52) DOE, U. S. D. o. E. *DOE/EIS-0391* **2012**, *Office of River Protection, U.S.*
747 *Department of Energy, Richland, WA*.
748 (53) Dayal, R.; Davis, R. E.; Schweitzer, D. G. *BNL-NUREG-33580* **1983**,
749 *Brookhaven National Laboratory, Upton, NY*.
750 (54) Allen, P. G.; Siemering, G. S.; Shuh, D. K.; Bucher, J. J.; Edelstein, N. M.;
751 Langton, C. A.; Clark, S. B.; Reich, T.; Denecke, M. A. *Radiochimica Acta* **1997**, *76*, 77.
752 (55) Duncan, J. B.; Cooke, G. A.; Lockrem, L. L. *RPP-RPT-29195* **2009**, *Washington*
753 *River Protection Solutions, Richland, WA, USA*.

754

755

756 **Figure Captions**

757 **Table 1** – Composition of the LAW Simulant utilized in Cast Stone formation.

758 **Table 2** – Composition of the simulated Hanford vadose zone pore water (VZPW) used in EPA
759 Method 1315 leach testing.

760 **Table 3** – Fabrication recipes for the Cast Stone samples used in this study.

761 **Figure 1** – the percentage of initial concentration of a) Tc (16 ppm) and b) Cr (873 ppm)
762 removed from the LAW simulant by the Tc getters prior to Cast Stone fabrication.

763 **Figure 2** – a) the resulting Tc D_{obs} measured and b) the resulting Na D_{obs} values during the 63 d
764 leaching period of the Cast Stone monoliths with and without Tc getters. The Cast Stone
765 monoliths were leached in VZPW and placed into a fresh leachant at each interval at a sample
766 surface area to leachate volume of $1 \text{ cm}^2 : 9 \text{ mL}$. The errors bars represent the standard deviation
767 of the mean on the two leaching samples.

768 **Figure 3** – photographs of the Cast Stone monoliths in their cured form, opened after curing and
769 following 63 d leaching for a) the control system with no getters, b) Sn-A containing Cast Stone
770 and c) KMS-2 containing Cast Stone.

771 **Figure 4** – a) photographs of the cross-sectioned pucks from the CS-Control monolith after 63 d
772 leaching in VZPW and before leaching and b) the corresponding iQid images showing Tc
773 distribution.

774 **Figure 5** – a) photographs of the cross-sectioned pucks from the CS-Sn-A monolith after 63 d
775 leaching in VZPW and before leaching and b) the corresponding iQid images showing Tc
776 distribution.

777 **Figure 6** – a) iQid image and photograph of the sample extracted from the CS-Sn-A, b)
778 magnified iQid image showing several Tc hot spots and the corresponding μ -XRF maps of c) Cr,
779 d) P and e) Sn. The white arrow in b) – e) highlights the same spot in each image.

780 **Figure 7** – a) photographs of the cross-sectioned pucks from the CS-KMS-2 monolith after 63 d
781 leaching in VZPW and before leaching and b) the corresponding iQid images showing Tc
782 distribution.

783 **Figure 8** – a) iQid image and photograph of the sample extracted from the CS-KMS-2, b)
784 magnified iQid image showing several Tc hot spots and the corresponding μ -XRF maps of c) Cr,
785 d) Sn and e) S.

786 **Figure 9** - Tc K-edge XANES spectrum and fit for the Cast Stone A) prior to leaching and B)
787 after 6 month leaching in VZPW. The corresponding table shows the Tc K-edge fitting results
788 for the Cast Stone samples analyzed. The numbers in parentheses represent the standard
789 deviations of the contribution of that component for the ending digit, p is the probability that
790 improvement of the fit, when this standard is included, is due to random error.

791

792

793

794

795